Research Square

Preprints are preliminary reports that have not undergone peer review.
They should not be considered conclusive, used to inform clinical practice,
or referenced by the media as validated information.

Asymmetric Driven Multispecies Reconnection Across a Strong Density Gradient at Mars

Laila Andersson

laila.andersson@lasp.colorado.edu

LASP, University of Colorado Boulder https://orcid.org/0000-0002-6384-7036

Stefan Eriksson

Laboratory for Atmospheric and Space Physics, University of Colorado Boulder https://orcid.org/0000-0002-5619-1577

Yuki Harada

Department of Geophysics, Graduate School of Science, Kyoto University https://orcid.org/0000-0002-4001-6352

Kathleen Hanley

University of California

James McFadden

University of California, Berkeley

Jacob Gruesbeck

NASA-GSFC

Jasper Halekas

University of Iowa

David Mitchell

Space Science Laboratory, University of California

Mahdi Benna

NASA

Shannon Curry

Laboratory for Atmospheric and Space Physics, University of Colorado, Boulder

Article

Keywords: Asymmetric Reconnection, plasma mixing, ionosphere, Mars

Posted Date: September 1st, 2026

DOI: https://doi.org/10.21203/rs.3.rs-10842339/v1

License: This work is licensed under a Creative Commons Attribution 4.0 International License.
Read Full License

Additional Declarations: There is **NO** Competing Interest.

Asymmetric Driven Multispecies Reconnection Across a Strong Density Gradient at Mars

Laila Andersson[1*], Stefan Eriksson[1†], Yuki Harada[2†], Kathleen G. Hanley[3], Jim P. McFadden[3], Jacob R. Gruesbeck[4], Jasper Halekas[5], David Mitchell[3], Mehdi Benna[6], Shannon Curry[1]

[1*]LASP, University of Colorado, Boulder,CO, USA.
[2]ISEE, Nagoya University, Nagoya, Japan.
[3]SSL, University of California, Berkeley, CA, USA.
[4]NASA Goddard Space Flight Center, Greenbelt, MD, USA.
[5] University of Iowa, Iowa, IA,USA.
[6] University of Maryland, Baltimore, MD,USA.

*Corresponding author(s). E-mail(s): laila.andersson@lasp.colorado.edu;
†Contributed to the interpretation of the event

Abstract

Reconnection observations involving large density gradients and multiple heavy-ion species are scarce, motivating the analysis of satellite observations at Mars. The analyzed event exhibits anti-parallel magnetic fields with a guide field, accompanied by a substantial density gradient of approximately one to two orders of magnitude involving multiple species: e^-, H^+, O^+, O_2^+, and CO_2^+. The event is examined in terms of the temporal and spatial scales of the heavy ions of an assumed reconnection event, with the expectation that the structure is maintained by electron currents. The distance between the shocked solar wind and the collision-dominated ionosphere–thermosphere is small compared with the characteristic lengths of the X-line and outflow region. The ionospheric ions are accelerated within the reconnection region but transition to predominantly outflow-directed motion outside the exhaust. Away from the X-line, a boundary layer forms populated by accelerated ionospheric ions. The observations suggest that multiple X-lines form within the same areographic region and collectively sustain the outflow region over an extended period. For each newly formed X-line, reconnection is proposed to advance to lower altitudes, locally eroding the Martian atmosphere. This event demonstrates that magnetic reconnection can efficiently exchange plasma between the solar wind and the Martian ionosphere.

Keywords: Asymmetric Reconnection, plasma mixing, ionosphere, Mars

1 Introduction

When two media with different properties are in contact, their separation is generally maintained by a balance of pressure forces. If this balance is disrupted, kinetic processes can become important and permit mixing across the interface. Magnetic reconnection is one such process, enabling plasma transport across otherwise distinct boundaries. Here, we present an event at Mars in which two plasma populations are observed to mix: warm H^+ originating from the solar wind (SW) and cold ionospheric O^+ and O_2^+ ions.

The investigated event is associated with a bifurcated magnetic field ($\mathbf{B}$) reversal and ion acceleration, both of which are characteristic signatures of magnetic reconnection. Gosling and Szabo (2008a). At Earth, reconnection has been observed in the magnetotail Petrukovich et al. (2016), at the magnetopause La Belle-Hamer et al. (1995a); Mozer et al. (2008); Stawarz (2024), and in the SW Gosling et al. (2005); Eriksson et al. (2022). In these environments, the plasma densities (n_e) on either side of the reconnection region are often comparable. An important exception is the magnetopause, where density ratios of up to $n_1/n_2 \sim 10$ can occur, with n_1 and n_2 denoting the plasma densities on opposite sides of the boundary. In the event examined here, however, the density gradient reaches $n_1/n_2 \sim 100$ when the boundary layer produced by the assumed reconnection process is included.

Mars provides a particularly unusual environment in which to study magnetic reconnection. The SW proton gyroradius, r_P, is comparable to the Martian radius (R_M), while the bow shock (BS) is located less than $1R_M$ above the planetary surface. These comparable spatial scales, together with the strong curvature of the interaction region, produce a highly dynamic and intrinsically three-dimensional system. In particular, the curvature of the Martian BS is significant and, unlike at Earth, the shock cannot always be approximated as a planar theoretical shock.

Because a theoretically well defined BS is difficult to identify at Mars, we refer to the region at and downstream of the nominal BS location as the turbulent solar wind (TSW). Within the TSW, the SW transitions from a cold, beam-like plasma into a warmer, decelerated population that is progressively diverted around Mars. Upstream of this region, ion–ion instabilities frequently generate perturbations with characteristic periods of 20–60sec Delva (2011); Halekas et al. (2017b); Turc (2025). These structures are then convected downstream with the SW at speeds exceeding 300km/sec. At such speeds, a perturbation travels a distance of $1R_M$ in approximately 10sec. Consequently, perturbations that reach the ionosphere are generally observed as discrete pulses.

At the opposite end of the interaction region lies the coupled ionosphere–thermosphere system. On the dayside, the peak Martian ionospheric density occurs at an altitude of approximately 150 km and rises to approximately 180–200 km toward the terminator Němec et al. (2017); Segale et al. (2024); Peter et al. (2025). At

these altitudes, the plasma is strongly controlled by the neutral thermosphere. Above approximately 180–250 km, the ion gyrofrequency begins to exceed the ion–neutral collision frequency Akbari et al. (2019). Nevertheless, significant ionosphere-thermosphere coupling can persist to altitudes of approximately 350 km.

On the dayside, where the solar zenith angle (SZA) is $< 45°$, the transition between the upper ionosphere and the TSW typically occurs at altitudes of approximately 400-500 km. However, this transition altitude varies substantially and is not determined solely by the prevailing SW conditions Lentz et al. (2021); Halekas et al. (2017a). The interaction is further complicated by the different characteristic velocities and spatial scales of the constituent ion species Holmberg et al. (2019). In the upper ionosphere, ions are demagnetized because $\mathbf{B}$ changes significantly over the scales equal to a gyroradii.

The dominant neutral species in the Martian thermosphere is CO_2, resulting in substantial CO_2^+ densities in the lower ionosphere. Although O_2^+ is generally the dominant ion species, its production occurs on timescales of tens of seconds to minutes, whereas O^+ can be produced within seconds and dominate the ion composition at higher altitudes. Consequently, the O^+/O_2^+ ratio varies with both altitude and the dynamical state of the ionosphere Andersson and Ergun (2012).

Mars lacks an intrinsic global $\mathbf{B}$; instead, its conductive ionosphere causes the interplanetary magnetic field (IMF) to drape around the planet. At low altitudes, the $\mathbf{B}$ orientation is therefore controlled primarily by the IMF Spreiter et al. (1970); Shaver et al. (2025). Under relatively stable upstream conditions, the $\mathbf{B}$ can diffuse into the collision-dominated ionosphere Cravens et al. (2023). The timescale required to establish a well-developed current system in the lower ionosphere, and the rate at which that system responds to changes in the IMF, remain poorly constrained. It is assumed an IMF-driven current system may be more readily established in the northern hemisphere, where the influence of crustal $\mathbf{B}$ is comparatively weak.

Magnetic reconnection has been modeled, studied in laboratory experiments, and observed in space for more than 50 years Kovalevsky (1971); Norgren (2025). However, the simultaneous observation of a $\mathbf{B}$ reversal and an ion jet is not, by itself, sufficient to demonstrate that reconnection is occurring. Drawing on studies at Earth Cassak and Shay (2007); Markidis et al. (2011), Figure 1a presents a simplified representation of asymmetric guide-field reconnection in LMN-coordinates Denton et al. (2018); Pritchett (2008).

The reconnection outflow has the characteristic speed related to the inflow Alfvén speed (v_A). In asymmetric reconnection, the exhaust structure is displaced toward one side of the current sheet Pritchett (2008), as indicated by the dashed line in Figure 1a. In a multispecies plasma, lighter ions such as H^+ respond more rapidly and may dominate the dynamics closer to the X-line, whereas heavier ion species become increasingly important farther downstream within the exhaust. The dominant contribution to the outflow is expected to originate from the high-density side.

Reconnection can extend over large distances along the outflow direction. The current-sheet width in the N-direction has been used to estimate the distance from the X-line along the L-direction Phan et al. (2007) . For a characteristic reconnection rate of 0.1, the ratio of current-sheet width to downstream distance is approximately

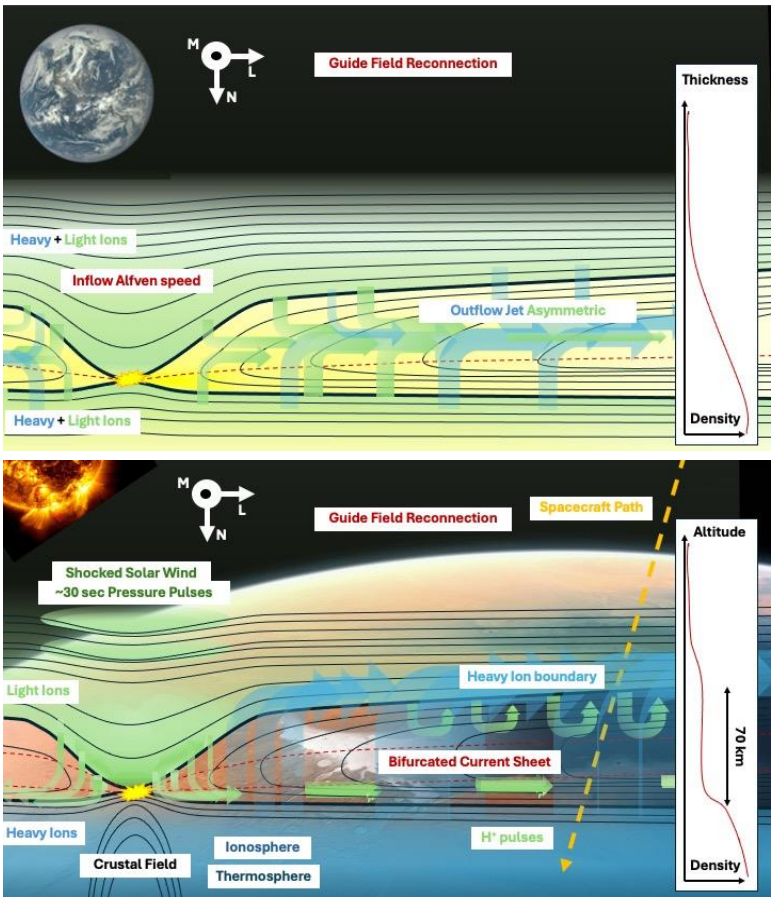


Fig. 1 Illustration of guide-field magnetic reconnection across a density gradient in a multispecies plasma. Panel (a) presents the current understanding derived primarily from observations and studies at Earth. Panel (b) illustrates the event investigated in this study, which occurs across a strong density gradient confined to a narrow altitude range along the N-direction. Images courtesy of NASA.

1:5. As reconnection continues, the current sheet may evolve through the formation of plasmoids in two dimensions or flux ropes in three dimensions, and the sheet may become bifurcated Daughton et al. (2004); Gosling and Szabo (2008a); La Belle-Hamer et al. (1995b). Bifurcation observations is more common observed in SW compare to Earth magnetopause and can be understood from the v_A on either side. The observed inflow difference in this event are more similar to the SW reconnection where clear current bifurcation is observed further support that this event is reconnection caused by draped IMF. Studies of driven current sheets have shown that electron temperature anisotropy and nongyrotropy can play important roles in the formation and interpretation of bifurcated current-sheet structures Ricci et al. (2004).

In space plasmas, the X-line has a finite extent in the M-direction and suggested to expand at a rate governed by the guide field v_A Shepherd et al. (2017). Accelerated

electrons are commonly observed along the separatrices Newman et al. (2022) and maintain **B** topology.

Reconnection at Mars has been proposed previously Dolginov and Zhuzgov (1991). Numerous studies have reported field-aligned ion flows that may be associated with reconnection Wang et al. (2023), however because v_A in the Martian ionosphere are relatively low any heavy ion flow cannot be used to identify reconnection. Ion beams have been interpreted as signatures of reconnection occurring in the TSW Harada et al. (2018a), entirely within the ionosphere Harada et al. (2018b), and even within the collision-dominated region Harada et al. (2025). Most previous investigations of reconnection at Mars have relied primarily on the coincident observation of ion jets and **B** reversals. The present study extends this earlier work by examining not only the characteristic signatures of reconnection but also the spatial structure, temporal evolution and multi-species of such process.

This investigation uses observations from NASA's Mars Atmosphere and Volatile EvolutioN (MAVEN) mission Jakosky et al. (2015). The MAVEN payload includes a magnetometer Connerney et al. (2015), a non-mass-resolving ion spectrometer Halekas et al. (2015), a mass-resolving ion spectrometer McFadden et al. (2015), an electron spectrometer Mitchell et al. (2016), a neutral and ion mass spectrometer Mahaffy et al. (2014), and a bulk-plasma instrument Andersson et al. (2015). Data from all of these instruments are used in the present investigation. The particle measurements are subject to several observational limitations, including restricted FOV, finite energy ranges, instrument operating modes, and variations in spacecraft potential. Where any of these factors may affect the interpretation, their possible influence is explicitly evaluated and discussed.

2 Results

2.1 Overview Of The Event

The event on 15 July 2021 was identified by a **B** reversal accompanied by a bifurcated current sheet, as shown in Figure 2. At approximately 20:30 UT, the spacecraft (SC) was located in the TSW at an altitude of ∼900km at a SZA of ∼23°. The event ended at approximately 20:50 UT, by which time the SC had entered the ionosphere–thermosphere region at an altitude of ∼230km, 68° North latitude, and an ∼80° SZA. The solid black vertical lines mark the outer boundaries of the reconnection interval and the bifurcated current sheet.

Before and after the event, the SW appeared relatively undisturbed based on observations near apoapsis (not shown). Prior to the event, the SW velocity was approximately 360km/sec in the antisunward direction. The IMF strength was ∼2nT, directed along $-B_{MSOx}$ and $-B_{MSOz}$, where the Mars-centered Solar Orbital (MSO) coordinate system is defined such that the (x)-axis points toward the Sun, the (z)-axis points northward out of the ecliptic plane, and the (y)-axis completes the right-handed coordinate system and points toward dusk. Following the event, at approximately 23:20 UT, the SW speed was ∼290km/sec, and **B** was ∼4nT with $+B_{MSOy}$ component dominating. These observations indicate that the IMF rotated by at least 90° over a period of approximately 2.5 hours.

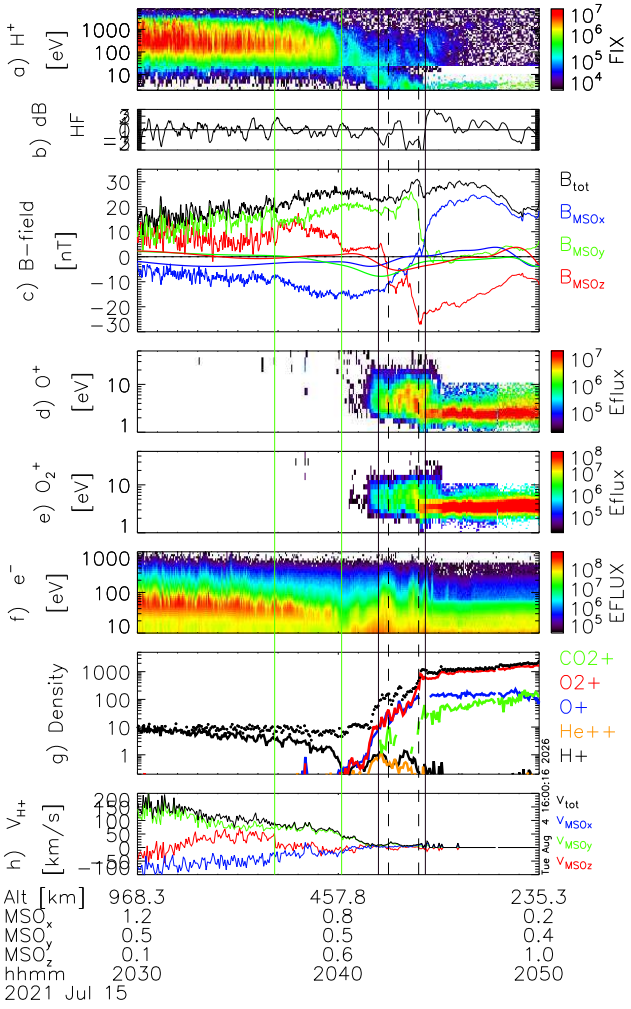


Fig. 2 Overview of the inbound MAVEN orbit on July, 15 2021. From top to bottom, the panels show H^+, dB, $\mathbf{B}$, O^+, O_2^+, e^-, n_p, and V_{H^+}, respectively. Changes within the magnetosheath are indicated by the green vertical lines, while the interval of interest is bounded by the black vertical lines.

The measured $\mathbf{B}$ and the modeled crustal $\mathbf{B}$ Langlais et al. (2019) are shown in F2c, while Figure 2b presents a filtered B_{MSOx} component. A $\mathbf{B}$ fluctuation with a characteristic period of $\sim 30 sec$ is observed in the TSW before approximately 20:36 UT. After approximately 20:46 UT, a fluctuation with a similar periodicity is observed in the ionosphere, while the original pulsation remains discernible, suggesting that the disturbance may have undergone mode conversion as it propagated into the ionospheric

plasma Collinson et al. (2018); Fowler et al. (2018). Throughout the event, $|\mathbf{B}|$ remains relatively constant.

In the TSW region, H^+ flows primarily in the $-v_{MSOx}$ and $+v_{MSOy}$ directions, as shown at the beginning of Figures 2a and 2h. On the ionospheric side, after approximately 20:44 UT, dispersed H^+ populations with energies above 25 eV are observed and are interpreted as a sequence of pulses recurring at intervals of approximately 30sec. These populations are inferred to originate in the TSW, become accelerated within a localized region into the ionospheric side, and subsequently propagate toward the SC. Each H^+ pulse spans a range of velocities, producing the observed overlapping energy-dispersed signatures. The velocity dispersion suggests that the acceleration region was located approximately 3000-5000 km from the SC.

Spectrograms of O^+, O_2^+, and e^- are shown in Figures 2d-f. After approximately 20:45 UT, the ion instrument transitions to a narrower energy-sweep range, as seen in Figures 2d and 2e. On the ionospheric side, accelerated heavy ions are observed between the two solid black vertical lines. Around 20:44 UT, the O^+ population exhibits a modulation with a characteristic period of ∼30sec, whereas no comparable modulation is evident in the heavier O_2^+ population.

The TSW region is characterized by hot electrons with energies below approximately 50 eV, together with the absence of significant heavy-ion populations and TSW extends to approximately 20:40 UT. Between the green and black vertical lines a heated electron population is observed. Immediately inside the black vertical lines, accelerated field-aligned electron populations are present. Adequate FOV coverage is available only near the first black vertical line. The locations of field-aligned electrons are consistent with the expected positions of the reconnection separatrices. Because the present investigation focuses on ion-scale processes, the electron observations are not analyzed further.

The density gradient measured by two of the instruments is shown in Figure 2g. The bulk plasma density is represented by the black dots, while the STATIC ion measurements are color-coded according to the legend. The bulk plasma density measurement becomes less sensitive at densities below approximately 10cm^{-3}. Despite differences in measurement technique, operating range, and FOV coverage, the three density measurements show that between approximately 20:40 and 20:45 UT, the measured plasma density changes by nearly two orders of magnitude.

At 20:30 UT, upstream of Mars, the plasma flow and $\mathbf{B}$ are shown in Figures 2c and 2h. In this H^+-dominated upstream region, v_A, ranges from approximately 100 to 600 km/s. At the first green vertical line, the flow speed decreases as the magnetic-field strength increases due to magnetic pileup. Between the green and black vertical lines, the H^+ flow speed decreases to approximately 10 km/s, while v_A decreases to approximately 12 km/s. On the ionospheric side, v_A falls below approximately 5 km/s.

For a reconnection event, the inflow v_A provides an upper limit on the characteristic outflow speed. Under the conditions observed during this event, the corresponding upper limits on the jet energies are approximately $2keV$ for H^+, $12eV$ for O^+, and $24eV$ for O_2^+.

2.2 The Reconnection Event

The **B** and ion velocities have been transformed into LMN-coordinate system and are shown in Figures 3a-c. The line styles are defined in the legend of each panel, and the solid and dashed black vertical lines mark the same boundaries identified in Figure 2. Outside the solid black vertical lines, B_L reverses from approximately $+22nT$ to $-28nT$, with a guide field of B_M~10-15nT. The nonmonotonic variation of B_L indicates a bifurcated current sheet Gosling and Szabo (2008b). Subtracting the weak crustal **B** does not alter this interpretation and is therefore not shown.

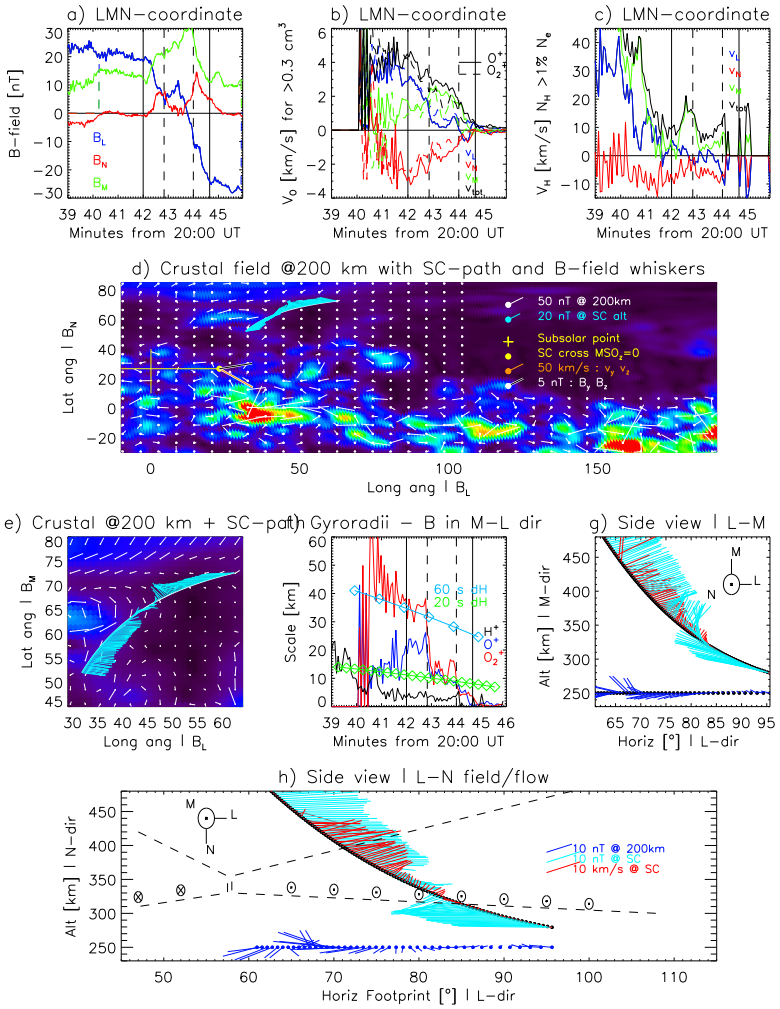


Fig. 3 The **B** , $v_{O^+}/v_{O_2^+}$, and v_{H^+} are presented in LMN coordinates in panels (a), (b), and (c), respectively. Panels (d) and (e) show the SC trajectory mapped to its aerographic footpoint, while panels (g) and (h) show the trajectory as a function of altitude, with the **B** vectors overlaid. See the text for further details.

During reconnection, lighter ions are expected to be accelerated closer to the X-line, whereas heavier ions respond farther downstream within the exhaust, as illustrated in Figure 1a Markidis et al. (2011). The warm TSW H^+ population is accelerated from the low-density side (before 20:40 UT), toward the high-density side (after 20:44 UT), producing the energy-dispersed signatures measured after ∼20:42 UT in Figure 2a. Reliable H^+ moments cannot be derived for the outflow in Figure 3c because of the low counting statistics, with H^+ accounting for less than 0.5% of the total plasma density. The observed H^+ energies remain below the upper limit set by the inflow v_A.

Reliable moments for the O^+ and O_2^+ populations are obtained when their densities exceed 0.3 cm^{-3}, as shown in Figure 3b. On the low-density side, both populations exhibit peak L-directed velocities below approximately 5km/sec, remaining below the inflow v_A. Between the solid black vertical lines, the O^+ and O_2^+ populations are continuously accelerated in the negative N-direction and subsequently redirected into the M- and L-directions by the **B**. This redirection is primarily controlled by the guide field, whereas between approximately 20:42 and 20:43 UT, the reconnecting **B** becomes the dominant influence. Owing to their large gyroradii, the heavy-ion populations begin to exhibit collective L-directed motion only outside the solid black vertical lines.

The primary acceleration of the TSW H^+ population is expected to occur near the X-line. Far from the X-line, however, the observed H^+ population on the low-density side is dominated by TSW H^+ reflected by the sharp magnetic-field gradient at the edge of the exhaust. The derived H^+ momentum therefore does not primarily represent the ion population accelerated near the X-line, but instead constitutes reflected TSW H^+. At large distances from the X-line, the exhaust may thus be maintained by the combined effects of the reconnection-associated electron population and gyrating TSW H^+. Once this ion boundary is established, the reflected TSW H^+ population, together with the heavy ions, may help sustain the exhaust structure as the reconnection dynamics evolve.

The vertical motion of the SC is the primary source of temporal variation in the observations. The relationship between the particle gyroradii, gyroperiods, and the altitude range traversed by the SC is evaluated in Figure 3f. The gyroradii of H^+, O^+, and O_2^+ are shown by the black, blue, and red lines, respectively. For a **B** strength of 25 nT, the corresponding gyroperiods are approximately 2, 40, and 80sec. The vertical distances traversed by the SC over 20 and 60sec are shown by the light-green and light-blue lines, respectively. On either side of the reconnection event, where the **B** is predominantly horizontal, the ion gyroradii are smaller than or comparable to the vertical distance traversed by the SC. Within the exhaust the SC traverses a vertical distance greater than that traveled by an ion over a gyroperiod. Consequently, the derived ion moments within the exhaust may not fully represent the local plasma distribution.

To better illustrate the mesoscale reconnection structure between approximately 20:40.5 and 20:46 UT, **B** vectors are superimposed on the SC trajectory using two different orbit projections. Figures 3d and 3e show the SC footprint on the Martian surface as a function of latitude and longitude, whereas Figures 3g and 3h show the SC altitude as a function of its horizontal aerographic footprint. In Figures 3d and 3h, the whiskers represent the B_N-B_L components, while in Figures 3e and 3g, they

represent the B_M-B_L components. The measured **B** vectors are shown in light blue, and the O^+ flow vectors are shown in red in Figures 3g and 3h. In Figure 3h, the dashed black line marks the approximate location of the reconnection separatrix.

The measured orbit information is presented together with the modeled crustal **B** at 200 km altitude Langlais et al. (2019). The crustal **B** strength is shown by the color map, while the horizontal field direction is indicated by white whiskers in Figures 3d and 3e. In Figures 3g and 3h, the crustal **B** is shifted to an altitude of 250 km and represented by dark-blue whiskers. In Figure 3d, the approximate subsolar point is marked by the large yellow cross, while the longitude at which the SC crosses from the southern to the northern MSO hemisphere ($z_{MSO} = 0$) is indicated by the yellow dot. At this location, the observed y_{MSO}-z_{MSO} component of **B** and v are shown according to the legend.

The crustal **B** near the SC trajectory are weak. The strongest crustal **B** is located well away from the observed path, as shown in Figure 3d. A relatively weak crustal **B** is present near latitudes of approximately 60°-65°, about one solar local time (SLT) hour earlier, as shown in Figure 3e. One SLT hour corresponds to 15° in longitude, or approximately 1000km at an altitude of 350km. The observed vertical thickness of the reconnection region is approximately 70km, as indicated by the dashed lines in Figure 3h. The H^+ velocity dispersion provided an upper limit of approximately 5000km to the X-line. Based on Figure 3e, the crustal field near 65° latitude and 30° longitude is approximately co-located with the inferred X-line position.

The SC traversed the reconnection region in approximately 150sec, corresponding to the interval between the black vertical lines in Figure 3a. During this interval, the SC moved horizontally by approximately 400km in the M-direction. Using the guide-field strength to estimate the v_A, and thus the characteristic X-line expansion rate, the X-line would expand from an initial point to a length of approximately 1500-4000km over 150sec. At an altitude of 350km, this distance corresponds to 1°–4°. In the projection shown in Figure 3e, the M-direction is most closely aligned with latitude. The observed latitudinal extent of approximately 5°–10° therefore exceeds that expected from expansion over the 150sec crossing interval, suggesting that reconnection had been active for several minutes before the SC entered the reconnecting region.

2.3 Reconnection Impact on Mars

To evaluate how reconnection between the TSW and ionosphere may affect the Martian plasma environment, altitude spectrograms from four consecutive days are presented in Figure 4. From top to bottom, the panels show the ion number flux integrated over $25eV$-$20keV$, **B**, modeled crustal **B**, n_e, and B_{MSOx} component. The white line in each panel marks the altitude at which the n_e decreases below 100 cm^{-3}, providing a useful proxy for the transition between the ionosphere and the TSW.

The black dashed line marks the orbit containing the reconnection event, while the white vertical lines identify orbits separated by approximately 24 hours, during which the SC passed over nearly the same aerographic region. During the event orbit, the transition between the ionosphere and the TSW occurred at an altitude more than 200km lower than during the other passes through this region. The proton flux shown

in Figure 4 does not indicate a corresponding enhancement in SW pressure, suggesting that the unusually low transition altitude was not driven by increased SW pressure.

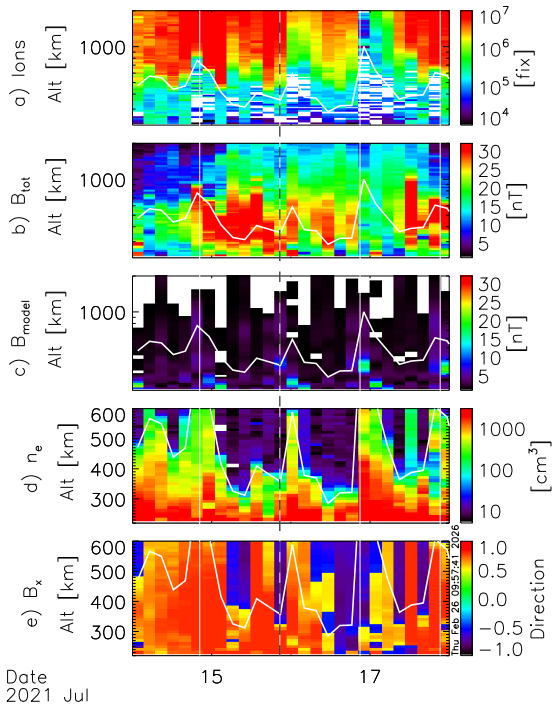


Fig. 4 Altitude profiles from four consecutive days of inbound orbital segments, illustrating the persistence of the event effects over several days. From top to bottom, the panels show the ion number flux integrated over $25eV$-$20keV$, the **B** strength, the modeled crustal **B** strength, the n_e, and variations in the B_x direction. The white curve overlaid on each panel marks the transition between ionosphere and TSW. The vertical white lines identify orbits separated by approximately 24 hours, while the dashed black line marks the orbit containing the reconnection event.

To assess whether the B_{MSOx} direction differs between the TSW and ionospheric regions, the color scale in Figure 4e is saturated to emphasize field reversals across the white line. Most orbits do not show a clear reversal across this boundary. Below the white line multiple field reversals are observed on many orbits, suggesting that a stable, large-scale ionospheric current system is not always present.

Under stable upstream conditions, the IMF direction can diffuse into the ionosphere and modify the ionospheric current system Cravens et al. (2023); Shaver et al. (2025). During the two orbits preceding the event orbit, the **B** direction remains relatively consistent above and below the white line, suggesting that sufficient time had elapsed for a large-scale ionospheric current system to develop. For the event orbit, the SC

first encountered a reversed B_{MSOx} at high altitude, whereas the ionospheric B_{MSOx} remained unchanged compared to previous orbits.

The **B** strength above the white line during the event orbit (Figure 4b) is also weaker than during the preceding orbits with comparable TSW ion fluxes (Figure 4a). This suggests that a well-developed magnetic pileup region had not yet formed, potentially allowing more direct coupling between the SW and the ionosphere. Taken together, these observations are consistent with a change in the IMF occurring after a large-scale ionospheric current system had already been established. Because the ionosphere could not adjust on the same timescale, the resulting **B** configuration may have produced the antiparallel geometry necessary for reconnection between the TSW and ionospheric plasma.

3 Discussion

Particle transit times provide an important constraint on the inferred spatial and temporal scales of the reconnection event. The overlapping dispersed H^+ signatures, recurring with a periodicity of ∼30sec, indicate a source region approximately 3000-5000km from the SC. Projecting this distance onto the L-direction suggests that the SC was located no more than approximately 3500km from the X-line. Electrons with energies of $50eV$ can traverse this distance in less than 1sec, which is shorter than the temporal resolution of the electron measurements.

A $2keV$ H^+ ion requires approximately 6sec to travel from the X-line to the SC. In contrast, ionospheric ions moving at less than 5km/sec cannot traverse the ∼70km exhaust thickness over the same interval. Assuming a mean velocity of 1.7km/sec (Figure 3b), O^+ and O_2^+ require approximately 40sec to cross the exhaust. Once redirected into the L-direction, the resulting O^+/O_2^+ jet can travel approximately 150km over 30sec.

The expected 5:1 ratio between the distance from the X-line and the current-sheet thickness does not appear to describe this event. One possible explanation is that the thermosphere acts as stiff boundary, limiting expansion in the N-direction, while the modulated downward pressure exerted by the TSW causing a driven reconnection event.

Based on the observed O^+/O_2^+ velocities, the mesoscale **B** structure was likely established >40sec before the SC reached the reconnecting **B** and persisted through the final dispersed H^+ signature. Reconnection therefore remained active for at least ∼7min. If the guide-field v_A of 10-15km/sec approximates the horizontal expansion speed of the X-line, a single X-line could have expanded by approximately 6000-10,000km over this interval, corresponding to an aerographic extent of ∼6°-11°. An X-line of this scale is consistent with the spatial extent illustrated in Figure 3e.

The ∼30sec modulation in TSW may cause the reconnection to pulsate or cause periodic creation of new X-lines. That individual X-lines located in vicinity of each other contributing to a global **B** topology has been observed Trattner et al. (2021). Although modulation of a single X-line cannot be excluded the multiple-X-line interpretation is more likely. Under this interpretation, the SC sampled the exhaust several

thousand kilometers downstream of a highly dynamic X-line region, where the plasma dynamics were increasingly controlled by the heavier slow moving ionospheric ions.

Modulation is observed in the O^+ inflow near 20:44 UT in Figure 2d but it is not evident in the O_2^+ population in Figure 2e. This difference likely reflects the different in two ion species speeds and the distances from the X-line. Closer inspection of the O^+ spectrogram reveals one, and possibly two, convective dispersions in which 2-3eV O^+ ions are observed before higher-energy ions at ∼5-10eV. Because the O_2^+ population is more than an order of magnitude denser than the O^+ population, O_2^+ is expected to dominate the ion dynamics within the exhaust.

The small vertical extent of the interaction region between the SW and the Martian surface, relative to R_M, may allow successive X-lines to form within a relatively limited aerographic region. Pressure pulses in the TSW can influence a broad horizontal region on the dayside, while the underlying thermosphere-ionosphere remains comparatively uniform. Under these conditions, the weak crustal **B** located upstream of the observation (Figure 3e) may provide a persistent localized perturbation that facilitates the onset of reconnection within a confined region. Each TSW pressure pulse may enhance the local pressure imbalance and trigger a new X-line within approximately the same aerographic region. Because the draped **B** is substantially stronger than the crustal **B** at the altitude of the X-line, the event is not interpreted as reconnection between the crustal **B** and the IMF. Instead, the crustal **B** may act as a localized catalyst for reconnection between the oppositely directed **B** above it.

Comparison with altitude profiles obtained over the same aerographic region (Figure 4) shows that the orbit of interest had substantially lower n_e between approximately 320 and 390km altitude. If the X-line region initially formed near 390km and successive reconnection episodes progressively moved downward toward 320km, the resulting process could erode the upper ionosphere. The inferred vertical displacement of approximately 70km would require about 20min, roughly twice the duration needed to account for the observed spatial extent of the reconnection event.

4 Conclusion

Observation of plasma exchange between the Martian ionosphere and the SW is presented. The event shown in Figure 2 is interpreted as driven, multispecies magnetic reconnection across a strong density gradient in the presence of a guide field, as illustrated in Figure 1b. The SC was located approximately 3500km downstream of the X-line, where the reconnection exhaust exhibited a bifurcated current sheet.

During the 6-10hours preceding the event, stable IMF conditions allowed a well-defined, large-scale ionospheric current system to develop. When the IMF subsequently changed direction, the ionosphere could not reorganize on the same timescale, resulting in an antiparallel **B** configuration between the ionosphere-dominated region and the TSW.

The downward pressure exerted by the TSW was modulated by pulses with a periodicity of ∼30sec. At the time of the event, a weak crustal **B** was located upstream of the observation region and may have provided a localized perturbation that facilitated

the formation of a new X-line during each pressure pulse. These repeated reconnection episodes produced H^+ injections into the ionosphere with a similar cadence. Because no strong horizontal boundary restricts exhaust expansion, and because the heavier ionospheric ions respond more slowly than electrons and protons, a large-scale reconnection exhaust developed over time and persist as successive X-lines form and dissipate.

The energy-dispersed H^+ jet, accelerated near the X-line, was observed on the high-density side of the current sheet indicating the progression of the X-line to lower altitudes and the erosion of the ionosphere. The slower ionospheric O^+ and O_2^+ populations which was observed by the SC entered the exhaust farther downstream, were accelerated across it, and subsequently redirected into the L-direction. The resulting heavy-ion jet became fully developed outside the central exhaust. This evolution produced strong plasma gradients far downstream of the X-line and led to the formation of an ion boundary on the low-density side, where the local TSW H^+ population was reflected. To the best of our knowledge, such a boundary has not previously been reported and may arise from the characteristic spatial and temporal scales of the Martian plasma environment. Based on all timescales, it is likely this reconnection event have been active for 20min.

Electrons and light ions likely initiate and initially drive the reconnection process. Once the heavier ionospheric ions become dynamically involved, their greater momentum allows them to increasingly control and sustain the large-scale reconnection exhaust. However, because of the low v_A in the ionosphere, reconnection is unlikely to be a major mechanism for accelerating ionospheric ions at Mars.

The significance of magnetic reconnection at Mars extends beyond the acceleration of individual particles. This event demonstrates that reconnection may (1) facilitate the exchange and mixing of SW and ionospheric plasma, (2) erode the upper ionosphere on timescales of minutes, and (3) accelerate SW H^+ into the ionosphere, where the particles may deposit energy in the thermosphere and contribute to atmospheric heating and auroral emissions Crismani et al. (2019).

Acknowledgments. The work in this investigation was supported by NASA through the Mars Exploration Program.

References

Akbari H, Andersson L, Peterson WK, et al (2019) Ambipolar electric field in the martian ionosphere: Maven measurements. Journal of Geophysical Research: Space Physics 124(6):4518–4524. https://doi.org/https://doi.org/10.1029/2018JA026325

Andersson L, Ergun R (2012) Neutral wind effects on ion outflow at mars. Earth, Planetary, and Space 64:105–112. https://doi.org/10.5047/eps.2011.06.047

Andersson L, Ergun R, Delory GT, et al (2015) The langmuir probe and waves (lpw) instrument for maven. Space Sci Rev https://doi.org/https://doi.org/10.1007/s11214-015-0194-3

Cassak PA, Shay MA (2007) Scaling of asymmetric magnetic reconnection: General theory and collisional simulations. Physics of Plasmas 14(10):102114. https://doi.org/10.1063/1.2795630

Collinson G, Wilson III LB, Omidi N, et al (2018) Solar wind induced waves in the skies of mars: Ionospheric compression, energization, and escape resulting from the impact of ultralow frequency magnetosonic waves generated upstream of the martian bow shock. Journal of Geophysical Research: Space Physics 123(9):7241–7256. https://doi.org/https://doi.org/10.1029/2018JA025414

Connerney J, Espley J, Lawton P, et al (2015) The maven magnetic field investigation. Space Sci Rev 195. https://doi.org/https://doi.org/10.1007/s11214-015-0169-4

Cravens TE, Hamil O, Renzaglia A, et al (2023) Fourier analysis of magnetic fields in the ionosphere of mars. Journal of Geophysical Research: Space Physics 128(4):e2022JA031044. https://doi.org/https://doi.org/10.1029/2022JA031044

Crismani MMJ, Deighan J, Schneider NM, et al (2019) Localized ionization hypothesis for transient ionospheric layers. Journal of Geophysical Research: Space Physics 124(6):4870–4880. https://doi.org/https://doi.org/10.1029/2018JA026251

Daughton W, Lapenta G, Ricci P (2004) Nonlinear evolution of the lower-hybrid drift instability in a current sheet. Phys Rev Lett 93:105004. https://doi.org/10.1103/PhysRevLett.93.105004, URL https://link.aps.org/doi/10.1103/PhysRevLett.93.105004

Delva MCBCM. (2011) Upstream ion cyclotron waves at venus and mars. Space Sci Rev https://doi.org/https://doi.org/10.1007/s11214-011-9828-2

Denton RE, Sonnerup BU Russell CT, et al (2018) Determining l-m-n current sheet coordinates at the magnetopause from magnetospheric multiscale data. Journal of Geophysical Research: Space Physics 123(3):2274–2295. https://doi.org/https://doi.org/10.1002/2017JA024619

Dolginov S, Zhuzgov L (1991) The magnetic field and the magnetosphere of the planet mars. Planetary and Space Science 39(11):1493–1510. https://doi.org/https://doi.org/10.1016/0032-0633(91)90077-N

Eriksson S, Swisdak M, Weygand JM, et al (2022) Characteristics of multi-scale current sheets in the solar wind at 1 au associated with magnetic reconnection and the case for a heliospheric current sheet avalanche. The Astrophysical Journal 933(2):181. https://doi.org/10.3847/1538-4357/ac73f6

Fowler CM, Andersson L, Ergun RE, et al (2018) Maven observations of solar wind-driven magnetosonic waves heating the martian dayside ionosphere. Journal of Geophysical Research: Space Physics 123(5):4129–4149. https://doi.org/https://doi.org/10.1029/2018JA025208

Gosling JT, Szabo A (2008a) Bifurcated current sheets produced by magnetic reconnection in the solar wind. Journal of Geophysical Research: Space Physics 113(A10). https://doi.org/https://doi.org/10.1029/2008JA013473, URL https://agupubs.onlinelibrary.wiley.com/doi/abs/10.1029/2008JA013473

Gosling JT, Szabo A (2008b) Bifurcated current sheets produced by magnetic reconnection in the solar wind. Journal of Geophysical Research: Space Physics 113(A10). https://doi.org/https://doi.org/10.1029/2008JA013473

Gosling JT, Skoug RM, McComas DJ, et al (2005) Direct evidence for magnetic reconnection in the solar wind near 1 au. Journal of Geophysical Research: Space Physics 110(A1). https://doi.org/https://doi.org/10.1029/2004JA010809

Halekas J, Taylor E, Dalton G, et al (2015) The solar wind ion analyzer for maven. Space Sci Rev 195. https://doi.org/https://doi.org/10.1007/s11214-013-0029-z

Halekas JS, Brain DA, Luhmann JG, et al (2017a) Flows, fields, and forces in the mars-solar wind interaction. Journal of Geophysical Research: Space Physics 122(11):11,320–11,341. https://doi.org/https://doi.org/10.1002/2017JA024772

Halekas JS, Ruhunusiri S, Harada Y, et al (2017b) Structure, dynamics, and seasonal variability of the mars-solar wind interaction: Maven solar wind ion analyzer in-flight performance and science results. Journal of Geophysical Research: Space Physics 122(1):547–578. https://doi.org/https://doi.org/10.1002/2016JA023167

Harada Y, Halekas JS, DiBraccio GA, et al (2018a) Magnetic reconnection on dayside crustal magnetic fields at mars: Maven observations. Geophysical Research Letters 45(10):4550–4558. https://doi.org/https://doi.org/10.1002/2018GL077281

Harada Y, Halekas JS, DiBraccio GA, et al (2018b) Magnetic reconnection on dayside crustal magnetic fields at mars: Maven observations. Geophysical Research Letters 45(10):4550–4558. https://doi.org/https://doi.org/10.1002/2018GL077281

Harada Y, Cravens TE, Brain DA, et al (2025) Exploring magnetic reconnection in the collisional ionosphere of mars with maven. Geophysical Research Letters 52(22):e2025GL118950. https://doi.org/https://doi.org/10.1029/2025GL118950, e2025GL118950 2025GL118950

Holmberg MKG, André N, Garnier P, et al (2019) Maven and mex multi-instrument study of the dayside of the martian induced magnetospheric structure revealed by pressure analyses. Journal of Geophysical Research: Space Physics 124(11):8564–8589. https://doi.org/https://doi.org/10.1029/2019JA026954

Jakosky B, Lin R, Grebowsky J, et al (2015) The mars atmosphere and volatile evolution (maven) mission. Space Sci Rev 195. https://doi.org/https://doi.org/10.1007/s11214-015-0139-x

Kovalevsky J (1971) The interplanetary medium and its interaction with the earth's magnetosphere. Space Sci Rev https://doi.org/https://doi.org/10.1007/BF00171764

La Belle-Hamer AL, Otto A, Lee LC (1995a) Magnetic reconnection in the presence of sheared flow and density asymmetry: Applications to the earth's magnetopause. Journal of Geophysical Research: Space Physics 100(A7):11875–11889. https://doi.org/https://doi.org/10.1029/94JA00969

La Belle-Hamer AL, Otto A, Lee LC (1995b) Magnetic reconnection in the presence of sheared flow and density asymmetry: Applications to the earth's magnetopause. Journal of Geophysical Research: Space Physics 100(A7):11875–11889. https://doi.org/https://doi.org/10.1029/94JA00969, URL https://agupubs.onlinelibrary.wiley.com/doi/abs/10.1029/94JA00969

Langlais B, Thébault E, Houliez A, et al (2019) A new model of the crustal magnetic field of mars using mgs and maven. Journal of Geophysical Research: Planets 124(6):1542–1569. https://doi.org/https://doi.org/10.1029/2018JE005854

Lentz CL, Baker DN, Andersson L, et al (2021) The effects of different drivers on the induced martian magnetosphere boundary: A case study of september 2017. Journal of Geophysical Research: Space Physics 126(2):e2020JA028105. https://doi.org/https://doi.org/10.1029/2020JA028105

Mahaffy P, Benna M, King T, et al (2014) Mhe neutral gas and ion mass spectrometer on the mars atmosphere and volatile evolution mission. Space Sci Rev 195. https://doi.org/https://doi.org/10.1007/s11214-014-0091-1

Markidis S, Lapenta G, Bettarini L, et al (2011) Kinetic simulations of magnetic reconnection in presence of a background o+ population. Journal of Geophysical Research: Space Physics 116(A1). https://doi.org/https://doi.org/10.1029/2011JA016429

McFadden J, Kortmann O, Curtis D, et al (2015) Maven suprathermal and thermal ion compostion (static) instrument. Space Sci Rev 195. https://doi.org/https://doi.org/10.1007/s11214-015-0175-6

Mitchell D, Mazelle C, Sauvaud Jea (2016) The maven solar wind electron analyzer. Space Sci Rev 200. https://doi.org/https://doi.org/10.1007/s11214-015-0232-1

Mozer FS, Pritchett PL, Bonnell J, et al (2008) Observations and simulations of asymmetric magnetic field reconnection. Journal of Geophysical Research: Space Physics 113(A1). https://doi.org/https://doi.org/10.1029/2008JA013535

Newman DL, Eriksson S, Lapenta G (2022) Tripolar guide magnetic fields due to island coalescence in solar wind current sheets: Simulation and theory. Physics of Plasmas 29(11):112905. https://doi.org/10.1063/5.0102906

Norgren CLGDeaC. (2025) Electron and ion dynamics in reconnection diffusion regions. Space Sci Rev https://doi.org/https://doi.org/10.1007/s11214-025-01197-z

Němec F, Morgan DD, Fowler CM, et al (2017) Ionospheric electron densities at mars: Comparison of mars express ionospheric sounding and maven local measurements. Journal of Geophysical Research: Space Physics 122(12):12,393–12,405. https://doi.org/https://doi.org/10.1002/2017JA024629

Peter K, Pätzold M, Withers P, et al (2025) The variability of the topside ionospheres of venus and mars as seen by recent radio science observations. Icarus 432:116469. https://doi.org/https://doi.org/10.1016/j.icarus.2025.116469

Petrukovich A, Artemyev A, Nakamura R (2016) Magnetotail Reconnection, Springer International Publishing, Cham, pp 277–313. https://doi.org/10.1007/978-3-319-26432-5_7

Phan TD, Drake JF, Shay MA, et al (2007) Evidence for an elongated (gt; 60 ion skin depths) electron diffusion region during fast magnetic reconnection. Phys Rev Lett 99:255002. https://doi.org/10.1103/PhysRevLett.99.255002, URL https://link.aps.org/doi/10.1103/PhysRevLett.99.255002

Pritchett PL (2008) Collisionless magnetic reconnection in an asymmetric current sheet. Journal of Geophysical Research: Space Physics 113(A6). https://doi.org/https://doi.org/10.1029/2007JA012930, URL https://agupubs.onlinelibrary.wiley.com/doi/abs/10.1029/2007JA012930

Ricci P, Lapenta G, Brackbill JU (2004) Structure of the magnetotail current: Kinetic simulation and comparison with satellite observations. Geophysical Research Letters 31(6). https://doi.org/https://doi.org/10.1029/2003GL019207

Segale J, Felici M, Withers P, et al (2024) Characterization of the m1 and m2 layers in the undisturbed martian ionosphere at a variety of solar conditions with maven rose. Icarus 424:116251. https://doi.org/https://doi.org/10.1016/j.icarus.2024.116251, URL https://www.sciencedirect.com/science/article/pii/S0019103524003117

Shaver SR, Andersson L, Ramstad R, et al (2025) Piercing the martian veil: A statistical study of interplanetary magnetic field reach through ionospheric pressure balance. Journal of Geophysical Research: Space Physics 130(2):e2024JA033254. https://doi.org/https://doi.org/10.1029/2024JA033254

Shepherd LS, Cassak PA, Drake JF, et al (2017) Structure of exhausts in magnetic reconnection with an x-line of finite extent. The Astrophysical Journal 848(2):90. https://doi.org/10.3847/1538-4357/aa9066, URL https://doi.org/10.3847/1538-4357/aa9066

Spreiter JR, Summers AL, Rizzi AW (1970) Solar wind flow past nonmagnetic planets—venus and mars. Planetary and Space Science 18(9):1281–1299. https://doi.org/https://doi.org/10.1016/0032-0633(70)90139-X, URL https://www.sciencedirect.com/science/article/pii/003206337090139X

Stawarz MPBNeaJ.E. (2024) The interplay between collisionless magnetic reconnection and turbulence. Space Sci Rev https://doi.org/https://doi.org/10.1007/s11214-024-01124-8

Trattner KJ, Fuselier SA, Petrinec SM, et al (2021) Long and active magnetopause reconnection x-lines during changing imf conditions. Journal of Geophysical Research: Space Physics 126(4):e2020JA028926. https://doi.org/https://doi.org/10.1029/2020JA028926, URL https://agupubs.onlinelibrary.wiley.com/doi/abs/10.1029/2020JA028926

Turc TKKPeaL. (2025) From foreshock 30-second waves to magnetospheric pc3 waves. Space Sci Rev https://doi.org/https://doi.org/10.1007/s11214-025-01152-y

Wang L, Huang C, Du A, et al (2023) Magnetic reconnection in the martian magnetotail: Occurrence rate and impact on ion loss. Geophysical Research Letters 50(18):e2023GL104996. https://doi.org/https://doi.org/10.1029/2023GL104996